Available online at www.sciencedirect.com
ScienceDirect
Journal of the European Ceramic Society 30 (2010) 3273–3282
www.elsevier.com/locate/jeurceramsoc

Critical energy for photopolymerization of ceramic suspensions in acrylate monomers

Vladislava Tomeckova, John W. Halloran *

University of Michigan, Ann Arbor, MI 48109-2136, USA

Received 17 March 2010; received in revised form 25 July 2010; accepted 2 August 2010
Available online 23 August 2010

Abstract

The critical energy dose E_c required for photopolymerization of silica and alumina suspensions in acrylate monomers was measured for a large series of suspensions, and contrasted with a model that based on the assumption that E_c is the dose necessary to exhaust the polymerization inhibitors. The major predictions of the model were in good agreement with the data: E_c is inversely proportional to photoinitiator concentration, directly proportional to inert dye concentration, and directly proportional to the concentration of inhibitors.

Keywords: Photopolymerization; SiO_2; Al_2O_3; Suspensions; Rapid prototyping

1. Introduction

Photopolymerizable ceramic suspensions have been widely used in many applications such as dental restoratives[1] or complex 3D ceramic objects built via ceramic stereolithography.[2,3]

Ceramic suspensions of powders in monomer solutions containing photoinitiators are photopolymerized by exposing the surface to actinic light, such as ultraviolet, at a dose E (J/m^2) that suffices to polymerize the suspension to a certain depth of cure C_d.[4] The cure depth is related to the logarithm of the energy dose[5] by $C_d = D_p \ln(E/E_c)$ where the photobehavior of the suspension is characterized by a critical energy E_c and a sensitivity D_p. The photobehavior parameters will depend upon the compositional variables in a ceramic suspension, which includes the amount and type of ceramic powder, the monomer solution, and the concentration and type of the photoactive agents, such as the photoinitiators, inert dyes, and polymerization inhibitors. In another paper,[6] we derived simple predictive models which relate the critical energy and resin sensitivity to the suspension composition, and presented a limited amount of data. In this paper we consider the critical energy model in more detail, contrast its predictions with experiment and evaluate the fundamental parameters and compositional variables that determine the critical energy. A companion paper[7] reports details on the sensitivity D_p.

Free-radical photopolymerization occurs when radicals created by the photoinitiator are present in sufficient quantity to initiate the polymerization reaction of the monomers.[8] However, monomers must be stable against small quantities of free radicals that might be inadvertently generated. Thus the monomer solutions contain inhibitors which are added to prevent an undesired reaction. Oxygen absorbed from the air can also behave as an inhibitor. The model for E_c was based on the presumption that for UV doses smaller than E_c, the free radicals created when a photoinitiator molecule absorbs a photon are consumed by inhibitors so polymerization does not occur. It also considers absorption of photons by inert dyes. The hypothesis of this model for critical energy is that E_c is given by the dose of UV photons that are not absorbed by inert dyes and produce a population of free radicals large enough to exhaust the population of inhibitors in the monomer solution to provide surplus free radicals to begin the polymerization reaction. The critical energy then depends upon the number and effectiveness of inhibitors that scavenge free radicals, the concentration and absorption coefficients of inert dyes that absorb photons, and the concentration and absorption coefficients of photoinitiators that create free radicals when they absorb photons. While it is the monomer suspension medium that is photo-chemically active, the pres-

* Corresponding author at: Department of Materials Science and Engineering, University of Michigan, 2300 Hayward Street, Ann Arbor, MI 48109-2136, USA. Tel.: +1 734 763 1051; fax: +1 734 763 4788.
E-mail address: peterjon@umich.edu (J.W. Halloran).

0955-2219/$ – see front matter © 2010 Elsevier Ltd. All rights reserved.
doi:10.1016/j.jeurceramsoc.2010.08.003

Nomenclature

C_d	cure depth
c_P	molar concentration of photoinitiator
c_D	molar concentration of dye
D_p	penetration depth
E_c	critical energy
ε_D	molar extinction coefficient of the dye
ε_P	molar extinction coefficient of the photoinitiator is ε_P
Φ	ceramic volume fraction
γ_D	the number of radicals that did not get generated because the photon was absorbed by an inert dye
γ_Q	potency of the inhibitor, or the number of radicals removed per inhibitor
γ_O	potency of the oxygen inhibitor, or the number of radicals removed per oxygen inhibitor
$h\nu$	photon energy
l_{Sc}	scattering length
O	concentration of oxygen inhibitor
Ω	quantum yield
Q	concentration of quinone-type inhibitor

ence of ceramic powders plays a passive role by diluting the active monomer, and an active role by limiting photon penetration depth by scattering. These effects were considered in an "inhibitor exhaustion model" for the critical energy parameter E_c which was derived in the previous paper.[6] The inhibitor exhaustion model suggests that the critical energy should depend on the compositional variables of the suspension, including the ceramic volume fraction Φ, the concentration of the photoinitiator (c_P in mol/L), the inert dye concentration (c_D in mol/L) and the concentration of quinone-type inhibitor (Q) and oxygen inhibitor (O), as:

$$E_c = (1-\Phi)\frac{h\nu}{\Omega}(\gamma_Q Q + \gamma_O O + \gamma_D c_D)\frac{1}{\varepsilon_P c_P} + \frac{h\nu}{\Omega}(\gamma_Q Q + \gamma_O O + \gamma_D c_D) \times \left[\frac{(1/l_{Sc}) + (1-\Phi)(\varepsilon_D c_D)}{(1-\Phi)\varepsilon_P^2}\right]\frac{1}{c_P^2} \quad (1)$$

The other terms in Eq. (1) are as follows: Ω is the quantum yield, or number of free radicals produced by absorption of a photon of energy $h\nu$; the molar extinction coefficient of the photoinitiator is ε_P; ε_D is the molar extinction coefficient of the dye; γ_Q is the potency of the inhibitor, or the number of radicals removed per inhibitor; and γ_O is the potency of the oxygen inhibitor, or the number of radicals removed per oxygen inhibitor; light scattering from the particles is characterized by the scattering length l_{Sc}.

Eq. (1) is written as a sum of terms linear in $1/c_P$ as the first term and terms quadratic in $1/c_P$ as the second term. It can be simplified if it happens that the quadratic term is much smaller than the linear term. If that is the case the quadratic term can be neglected, and the critical energy can be approximated in a linearized form:

$$E_c = (1-\Phi)\frac{h\nu}{\Omega}(\gamma_Q Q + \gamma_O O + \gamma_D c_D)\frac{1}{\varepsilon_P c_P} \quad (2)$$

The linearized form of the inhibitor exhaustion model makes several predictions that can be easily tested. It predicts that the critical energy should depend on the inverse of photoinitiator concentration as $1/c_P$, so that higher PI concentration should have smaller critical energy. A plot of E_c vs. $1/c_P$ should be straight line with zero intercept whose slope (K_3 in J-mol/m^2 L) reports the values of the terms in Eq. (3):

$$\frac{dE_c}{d(1/c_P)} = K_3 = (1-\Phi)\frac{h\nu}{\Omega}(\gamma_Q Q + \gamma_O O + \gamma_D c_D)\frac{1}{\varepsilon_P} \quad (3)$$

Eq. (2) also predicts that a plot of E_c vs. inert dye concentration should be linear. The intercept (I_4) should be given by Eq. (4a) and the slope (K_4 in J-L/m^2 mol) by Eq. (4b):

$$E_{c\ for(c_D=0)} = I_4 = (1-\Phi)\frac{h\nu}{\Omega}(\gamma_Q Q + \gamma_O O)\frac{1}{\varepsilon_P c_P} \quad (4a)$$

$$\frac{dE_c}{dc_D} = K_4 = (1-\Phi)\frac{h\nu}{\Omega}\frac{\gamma_D}{\varepsilon_P c_P} \quad (4b)$$

The critical energy should increase linearly with additions of inhibitors. Since there is an unknown amount of pre-existing inhibitor (Q_{native}), the total inhibitor concentration has both the native and added inhibitor, so we expect a plot of E_c vs. Q_{added} to have a slope (K_5) and intercept (I_5) given by Eqs. (5a) and (5b):

$$\frac{dE_c}{dQ_{added}} = K_5 = (1-\Phi)\frac{h\nu}{\Omega}\frac{\gamma_{Q,added}}{\varepsilon_P c_P} \quad (5a)$$

$$E_{c\ for(Q_{added}=0)} = I_5 = (1-\Phi)\frac{h\nu}{\Omega}(\gamma_{Q,native}Q_{native} + \gamma_O O + \gamma_D c_D)\frac{1}{\varepsilon_P c_P} \quad (5b)$$

The linearized inhibitor exhaustion model also predicts that the only effect of the ceramic comes from the volume fraction term, so E_c vs. the volume fraction ceramic should have a slope and intercept from Eqs. (6a) and (6b):

$$\frac{dE_c}{d\Phi} = K_6 = -\frac{h\nu}{\Omega}(\gamma_Q Q + \gamma_O O + \gamma_D c_D)\frac{1}{\varepsilon_P c_P} \quad (6a)$$

$$E_{c,\Phi=0} = I_6 = \frac{h\nu}{\Omega}(\gamma_Q Q + \gamma_O O + \gamma_D c_D)\frac{1}{\varepsilon_P c_P} \quad (6b)$$

so the slope and intercept should be *numerically equal*. Another prediction of the linearized model is that *all ceramics should behave similarly*. This is a consequence of neglecting the quadratic terms in Eq. (1), which contained the scattering length, which depends on the volume fraction, particle size and refractive index contrast. Different ceramic powders can have quite different values for the scattering length,[9,10] but since this term is not included in the simple linearized model, we expect strong

scattering powders (like alumina) to be have similarly as weakly scattering powders (like silica).

In this paper, we will test the predictions of the simple linearized model with experimental measurements of E_c varying the concentrations of photoinitiators, dyes, and inhibitors. Note that the terms in Eqs. (3)–(6) for the slopes and intercept appear repeatedly, so each independent series of experiments provides another value for these collections of terms. We will seek a self-consistent set of terms to enable us to predict the properties of unknown suspensions from the experimentally determined E_c values of tested suspensions. Some of the parameters can be independently measured, such as the molar extinction coefficients for the dye and the photoinitiator, which can be determined with spectrophotometry. We will compare a limited number of ceramic volume fractions with silicon dioxide suspensions, and present a small amount of data on aluminum oxide suspensions, and discuss the successes and limitations of the linearized inhibitor exhaustion model.

2. Experimental procedure

2.1. Method for determining critical energy

The critical energy was determined measuring the cure depth as a function of energy dose. The surfaces of photosuspensions were exposed to six different energy doses to make thin coupons of solid green ceramic. The energy doses ranges were chosen mostly with respect to the concentration of PI and dye. For example 60 vol% SiO_2 suspension with ketone PI and no dye was polymerized using the energy range 60–400 mJ/cm^2, while for example 55 vol% Al_2O_3 suspension with 0.0252 mol/L (wrt monomer) ketone PI and 0.0026 mol/L (wrt monomer) triazole dye required much higher energy doses ~500–3300 mJ/cm^2. The coupons were lifted from the liquid photosuspensions and rinsed with isopropanol to remove uncured suspension. The cured thickness C_d was measured with a micrometer on 5 different spots of the sample. For the E_c calculation, the minimum value was used. This approach minimizes errors that can arise due to improper cleaning technique and warping of the sample due to polymerization shrinkage. Each composition was measured ~2–3 times. The cure depths were on the order of mm in case of silica suspension with no dye or tens to hundreds of microns in case of Al_2O_3 suspension with dye. Coupons with smaller cure depths were more difficult to handle and had more variation.

The cure depths were plotted against the logarithm of the energy dose. A linear regression line was fit through the data set to infer the sensitivity D_p from the regression slope. The regression line was extrapolated to the $C_d = 0$ to infer E_c from the intercept. As it involves extrapolation on a semi-log plot with six points, the values of E_c determined were quite sensitive to the details of the regression line. The standard errors for the slope D_p and intercept $\ln(E_c)$ were estimated from the residual sum of squares, using a statistical analysis package (OriginPro 8, OriginLab Corporation, North Hampton, MA, USA) to estimate the average $\ln(E_{c\,average})$ and the residual sum of squares to estimate of the standard deviation of the $\ln(E_c)$ as $\delta \ln(E_c)$. When these are expressed as E_c rather than $\ln(E_c)$, the error limits are quite asymmetric, so are reported as $E_{c\,average}$ with limits $E_{c\,min}$ and $E_{c\,max}$.

Most photopolymerization experiments were performed by laser scanning in a stereolithography apparatus (SLA-250, 3D systems, Inc., Valencia, CA, USA) with a solid state laser (Xcyte, JDSU, Milpitas, CA, USA), that had a quasi-continuous wave emitting at 355 nm, output power 30 mW, and a beam diameter of 125 μm. The intensity of the laser beam was measured before each experiment using the sensor built into the SLA-50, which had been calibrated with a thermal laser power meter (Orion-TH, Ophir Optronics, Jeruselem, Israel). A standard SLA test protocol was used to vary the dose by changing the scanning rate and hatch spacing. Other experiments were preformed using a UV curing apparatus (Conveyorized UV Curing System, Hanovia, Newark, NJ, USA) equipped with 300 W mercury vapor lamps. Hanovia lamps have strong lines at 305, 315, 365, 405 and 415 nm. The UV exposure dose was calibrated using a radiometer (UV-integrator PC-2008, Hanovia).

2.2. Materials

2.2.1. Photoactive agents

Photopolymerizable suspensions in this study are based on photocurable monomers 1,6-hexanediol diacrylate (SR238, Sartomer, USA) and ethoxylated pentaerythritol tetraacrylate (SR494, Sartomer, USA). Both are fast curing acrylate monomers and were used as-received. The diacrylate is a bifunctional monomer of low viscosity (9 mPa s), density 1.02 g/cm^3, molecular weight 226 g/mol and provides hardness when polymerized. The tetraacrylate has viscosity 108 mPa s, density 1.128 g/cm^3 and molecular weight 528 g/mol.

The photoactive agents included free-radical producing photoinitiators and inert absorbing dyes. The photoinitiator used for most experiments was a non-photobleaching ketone (Irgacure 184, Ciba, USA). Irgacure 184 is 1-hydroxy-cyclohexyl-phenyl-ketone and is a solid white powder with density 1.1–1.2 g/cm^3. Some experiments were conducted with a photobleaching phosphine oxide photoinitiator (Irgacure 819, Ciba, USA). Irgacure 819 is phosphine oxide, phenylbis(2,4,6-trimethyl benzoyl). It is a solid light yellow powder with density 1.205 g/cm^3. The inert UV dye was a commercial UV absorber (Tinuvin 171, Ciba, USA). Tinuvin 171 belongs to the hydroxyphenylbenzotriazole class and its main component is phenol, 2-(2H-benzotriazol-2-yl)-6-dodecyl-4-methyl-, branched and linear. It is a yellow liquid with pH 5.4 and density 1.003 g/cm^3. A visible dye, Thermoplast yellow 104 (BASF, USA) was used as a "blue light absorber". It is 3H-pyrazol-3-one,4-[(1,5-dihydro-3-methyl-5-oxo-1-phenyl-4H-pyrazol-4-ylidene)methyl]-2,4-dihydro-5-methyl-2-phenyl. It is a yellow powder and exhibits good solubility in these acrylate monomers. The absorbance spectra for all the photoactives are reported in a companion paper,[7] where we also report values of the molar absorption coefficients obtained by convoluting the absorption spectra with the emission lines of the laser (355 nm) and the emission spectrum of the mercury vapor lamps.

Table 1
Properties of used photoinitiators, dyes, radical scavengers and inhibitors.

	Commercial name	Density (g/cm^3)	Molecular weight (g/mol)
Photoinitiator	Irgacure 184	1.1–1.2	204.3
Photoinitiator	Irgacure 819	1.205	418.5
UV light absorber	Tinuvin 171	1.003	~395
Visible light absorber	Thermoplast yellow 104	1.3	358.5
HALS stabilizer	Tinuvin 123	0.97	737
HALS stabilizer	Irgastab UV 10	1.12	510.7
Inhibitor	Methoxy hydroquinone	–	140.14

Two types of inhibitors were used to as radical scavengers. Two were commercial hindered amine light stabilizers (HALSs) (Tinuvin 123 and Irgastab UV 10, Ciba, USA). Tinuvin 123 was a clear, slightly yellow liquid exhibiting viscosity ~3 Pa s at 20 °C. Irgastab UV 10 is an orange crystalline powder and has density 1.12 g/cm^3. The other inhibitor was methoxy hydroquinone (2,5-dihydroxyanisol, Sigma–Aldrich, USA) and was used as inhibitor. Table 1 summarizes the properties of the photoinitiators, dyes, radical scavengers and inhibitors.

2.2.2. Ceramic suspensions

The ceramic powder was silicon oxide, 99.8%, metal basis (Alfa Aesar, USA). This is a fused silica with mean diameter 7.1 μm, a specific area of 5 m^2/g and density 2.2 g/cm^3 (all from the manufacturer's specifications) and was used as-received without further purification. Alumina powder (A16-SG, Alcoa, USA) with particles mean diameter $d_{50} = 0.4$ μm, specific surface area 8.6 m^2/g and density 3.92 g/cm^3 (from the manufacturer's specifications) was used as-received without further purification. The colloidal dispersant for these powder in the acrylate monomers was a commercial alkoxylated ammonium phosphate dispersant (Variquat CC-59, Evonik Degussa GmbH). The dispersant loading was 2.083 wt% with respect to the dry powder mass.

The ceramic suspensions were prepared by the ball milling. First, alumina milling media (1/4 in. diameter) were added into an opaque polyethylene bottle (size 250 mL) in the amount of 1/15 of the total volume of the bottle. The diacrylate and tetraacrylate monomers were added at the volume ratio 9/1 along with the dispersant. The mixture was ball milled for ~15 min at 30 rpm to produce a well blended system. Ceramic powder was added incrementally – one quarter at a time and after each powder addition the suspension was ball milled for at least 3 h. When desired vol% solid loading was achieved, the suspensions were ball milled additional 24 h. Photoinitiator was added last and suspensions were ball milled for other 6 h. In case of suspensions containing UV absorber, HALS stabilizer or inhibitor, these were added last and ball milled for one additional day. The total volume of the suspension was calculated to be one half of the total volume of the bottle.

3. Results

To understand critical energy and accuracy of the measurements, raw cure depth measurements data have to be explained first. Shown in Fig. 1 is the cure depth C_d vs. energy dose logarithm for 60 vol% SiO_2 suspension with ketone PI (0.2016 mol/L wrt monomer) and no dye. The graph contains 3 sets of cure depth-energy dose data, when each of the set includes 6 measurements at different energy dose. As can be seen from the graph, polymerization using the same energy dose results in variations in the C_d value. The variations in C_d are caused by several factors such as laser intensity fluctuations within 5–10%, accuracy of samples cleaning, accuracy of the micrometer and thickness measurement error.

According to Jacob's equation, the data can be fitted with linear regression line for C_d vs. ln(E), where the slope represents the sensitivity D_p and the x-intercept represents the critical energy E_c. Thus, average D_p and average E_c are obtained. Using a standard analysis of the linear regression with 95% confidence of interval, the variations in the penetration dept δD_p and critical energy δE_c can be determined. The variations in the D_p are within ±5%. On the other hand, E_c is "measured" by extrapolating the linear curve on a semi-log plot. Therefore the experimental determination of the critical energy by itself is not particularly accurate resulting in significantly larger errors as can be seen in Fig. 1. Moreover, the error bars are asymmetric because of the logarithm and they become more apparent when higher critical energy doses are required. Error bars were calculated on each individual composition.

The critical energy E_c was determined on a large series of suspensions with varying ceramic volume fraction, photoinitiator and dye concentration in order to test the proposed model. The linearized inhibitor exhaustion model predicts that E_c plotted against $1/c_P$ should be a straight line with zero intercept. We expect E_c to decrease with increasing photoinitiator concentration. The slope should be steeper with lower ceramic volume, larger inhibitor or dye concentration. To test these predictions, the critical energy of a series of suspensions was plotted against

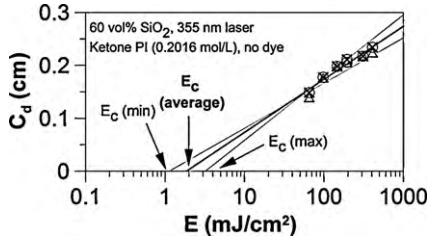

Fig. 1. Cure depths vs. energy dose for 60 vol% SiO_2 suspension with ketone PI (0.2016 mol/L) and no dye. Cure depth measurements were performed using 355 nm laser. The data was fitted with $y = K.\ln x + q$, where the slope represents sensitivity D_p and the x-intercept the critical energy E_c. The average energy is 1.89 mJ/cm^2, E_{min} = 1.19 mJ/cm^2 and E_{max} = 3.28 mJ/cm^2.

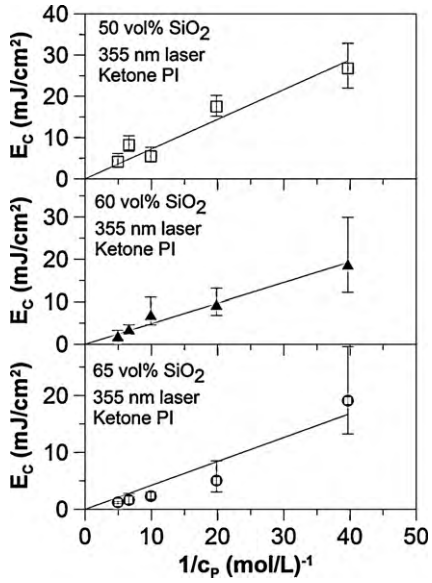

Fig. 2. Critical energy vs. $1/c_P$ for 50, 60 and 65 vol% SiO_2 suspensions with ketone PI and no dye.

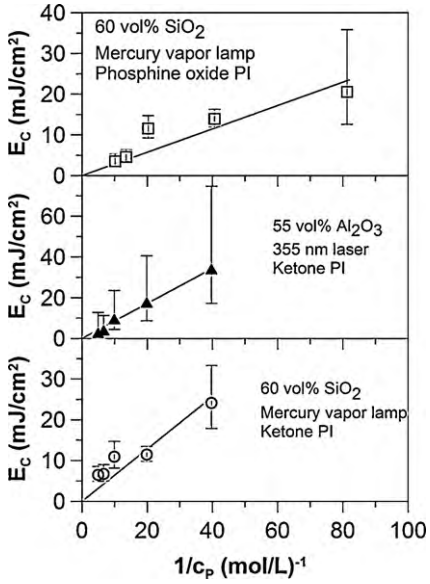

Fig. 3. Critical energy vs. $1/c_P$ for 60 vol% SiO_2 suspensions with the ketone and phosphine oxide PI and 55 vol% Al_2O_3 suspension with the ketone PI. Suspensions were prepared with no dye.

$1/c_P$ and fitted with linear regression with intercept forced to have zero intercept.

Shown in Fig. 2 are a series of plots of E_c vs. $1/c_P$ for 50, 60 and 65 vol% SiO_2 suspensions with ketone PI polymerized using the 355 nm laser. Similarly, shown in Fig. 3 is the E_c vs. $1/c_P$ for SiO_2 suspensions with the ketone PI and phosphine oxide PI polymerized using the mercury vapor lamp and Al_2O_3 suspensions with ketone PI polymerized using the 355 nm laser. The suspensions contain no dye ($c_D = 0$). In all cases, the data was satisfactory represented by a straight line with zero intercept. It appears that the prediction that $E_c \sim 1/c_P$ agrees with these observations. Consider now the actual slopes, which are presented in Table 2. In case of the silica suspensions with ketone PI polymerized using 355 nm laser, the slope increases with decreasing ceramic volume content as the model predicts. The slope term $K_3/(1-\Phi)$ should be the same for all compositions containing the same PI since the suspensions are based on the same monomer solution and contain similar concentration of the "native" inhibitors. The slope term $K_3/(1-\Phi)$ for suspensions with the ketone PI were roughly the same. The all in the range from 0.7 to 1.76 (mJ-mol)/(L-cm^2), with an average of 1.4 (mJ-mol)/(L-cm^2). Suspensions with the phosphine oxide PI had the $K_3/(1-\Phi)$ term of 0.89 (mJ-mol)/(L-cm^2).

The addition of an inert dye increases the critical energy. The E_c vs. $1/c_P$ curves for 60 and 50 vol% SiO_2 suspensions with triazole dye is shown in Figs. 4 and 5, respectively. The suspensions contain ketone PI and were polymerized using 355 nm laser. Again the critical energy values are represented well by a straight line with zero intercept. The actual slopes and correlation coefficients for individual compositions with the triazole dye are summarized in Table 3. From Eq. (3), we expect that the slope term $K_3/(1-\Phi)$ should increase with the concentration of inert dye. That is what is observed for the first 3 dye concentrations, but the slope term is smaller for the highest dye concentration. By excluding the portion of the energy consumed by the quinone inhibitor and oxygen inhibition determined previously (~1.39 (mJ-mol)/(L-cm^2)), the dye term $(h\nu/\Omega)(\gamma_D/\varepsilon_P)$ was estimated to be 1530 mJ/cm^2.

The simple linear model also predicts that, for a fixed concentration of photoinitiator, the critical energy dose should be a linear function of the inert dye concentration c_D. The slope and intercept of a plot of E_c vs. c_D should *decrease* with increasing PI concentration. Fig. 6 shows E_c vs. dye concentration for 50–65 vol% SiO_2 with ketone PI and triazole dye polymerized using 355 nm laser. The cure depth measurements were per-

Table 2
Actual slopes and correlation coefficients of linear regressions E_c vs. $1/c_P$ for SiO_2 and Al_2O_3 suspensions with no dye ($c_D = 0$). Intercept was set to zero.

Light source	Ceramic	PI	Φ	r^2	K_3	$\frac{K_3}{1-\Phi} = \frac{h\nu}{\Omega}(\gamma_Q Q + \gamma_O O)\frac{1}{\varepsilon_P}\frac{K_3}{(1-\Phi)} = \frac{h\nu}{\Omega}\left(\gamma_Q Q + \gamma_O O\right)\frac{1}{\varepsilon_P}$ (mJ-mol)/(L-cm^2)
355 nm laser	SiO_2	Ketone	0.5	0.94	0.785 ± 0.088	1.57 ± 0.18
	SiO_2		0.6	0.98	0.499 ± 0.100	1.25 ± 0.25
	SiO_2		0.65	0.99	0.248 ± 0.026	0.71 ± 0.07
	Al_2O_3		0.55	0.95	0.794 ± 0.552	1.76 ± 1.23
Mercury vapor lamp	SiO_2	Ketone	0.6	0.9	0.666 ± 0.085	1.66 ± 0.21
Average						1.39
Mercury vapor lamp	SiO_2	Phosphine oxide	0.6	0.95	0.357 ± 0.047	0.89 ± 0.12

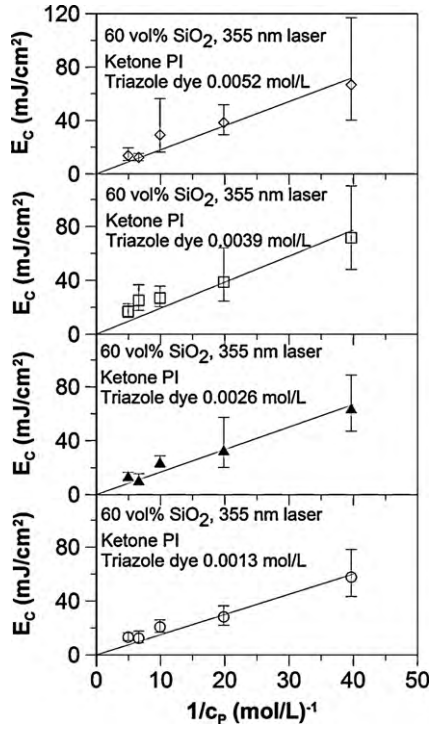

Fig. 4. Critical energy vs. $1/c_P$ for 60 vol% SiO_2 suspensions with ketone PI and varying concentration of triazole dye (wrt monomer).

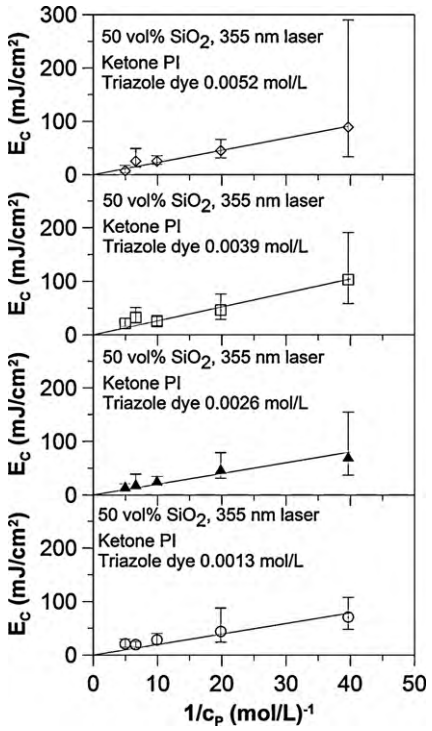

Fig. 5. Critical energy vs. $1/c_P$ for 50 vol% SiO_2 suspensions with ketone PI and varying concentration of triazole dye (wrt monomer).

formed using the 355 nm laser. Fig. 7 has data for 55 vol% Al_2O_3 suspensions with ketone PI, cure depth measurements were performed using the 355 nm laser. Fig. 7 also has data for 60 vol% SiO_2 with phosphine oxide PI (0.0984 mol/L wrt monomer) and blue light absorber (cure depth measurements performed using mercury vapor lamp). For clarity, the data in the graph are shown without error bars, although the linear regression lines considered the variations in E_c. Within some scatter, the critical energy increases linearly with inert dye concentration. The correlation coefficients, slopes and intercepts are shown in Table 4. Fig. 8 shows $I_4/(1-\Phi)$ vs. $1/c_P$ and $K_4/(1-\Phi)$ vs. $1/c_P$ for 50, 60 and 65 vol% SiO_2 suspensions. Both terms linearly increase with increasing PI concentration, which is in good agreement with the models prediction. Further, the intercept term $I_4c_P/(1-\Phi)$ should be the same for all compositions (with the same PI), since the compositions are based on the same monomer solution and therefore contain the same amount of the native inhibitors. Table 4 shows that for suspensions with the ketone photoinitiator this intercept term $I_4c_P/(1-\Phi)$ varied from about 0.7–2.7 (mJ-mol)/(L-cm^2) with an average around 1.45 (mJ-mol)/(L-cm^2). The intercept term was 0.96 (mJ-mol)/(L-cm^2) for suspensions with phosphine oxide PI. The dye term $(h\nu/\Omega)(\gamma_D/\varepsilon_P)$ was estimated to be 1400 mJ/cm^2, which agrees with the dye term determined from Table 3.

The intercept term $I_4c_P/(1-\Phi)$ from the dye concentration series of experiments (Table 4) should be numerically equal to the slope term $K_3/(1-\Phi)$ for suspensions with no dye from the PI concentration series of experiments (Table 2). In fact, these are in good agreement. For the ketone PI, the average value of $I_4c_P/(1-\Phi)$ is 1.45 (mJ-mol)/(L-cm^2), while the average value of $K_3/(1-\Phi)$ is 1.39 (mJ-mol)/(L-cm^2). For the phosphine PI, the values are 0.96 (mJ-mol)/(L-cm^2) from Table 4 and 0.89 (mJ-mol)/(L-cm^2) from Table 2.

Table 3
Actual slopes and correlation coefficients of linear regressions E_c vs. $1/c_P$ for 50 and 60 vol% SiO_2 suspensions with ketone PI and triazole dye.

Light source	Ceramic	Φ	c_D (mol/L)	r^2	K_3	$\frac{K_3}{1-\Phi} = \frac{h\nu}{\Omega}(\gamma_Q Q + \gamma_O O + \gamma_D c_D)\frac{1}{\varepsilon_P}\frac{K_3}{(1-\Phi)} = \frac{h\nu}{\Omega}\left(\gamma_Q Q + \gamma_O O + \gamma_D c_D\right)\frac{1}{\varepsilon_P}$ (mJ-mol)/(L-cm^2)	$\frac{h\nu}{\Omega}\frac{\gamma_D}{\varepsilon_P}$ (mJ/cm^2)
355 nm laser	SiO_2	0.6	0.0013	0.93	1.77 ± 0.24	4.4 ± 0.61	2300 ± 300
			0.0026	0.94	2.16 ± 0.29	5.4 ± 0.72	1550 ± 200
			0.0039	0.92	2.57 ± 0.50	6.4 ± 1.26	1300 ± 250
			0.0052	0.97	1.97 ± 0.35	4.9 ± 0.9	700 ± 100
	SiO_2	0.5	0.0013	0.92	2.64 ± 0.53	5.3 ± 1.0	3000 ± 600
			0.0026	0.98	2.77 ± 0.53	5.6 ± 1.0	1600 ± 300
			0.0039	0.89	2.93 ± 0.75	5.9 ± 1.5	1150 ± 300
			0.0052	0.96	2.36 ± 0.68	4.7 ± 1.4	600 ± 200
Average							1530

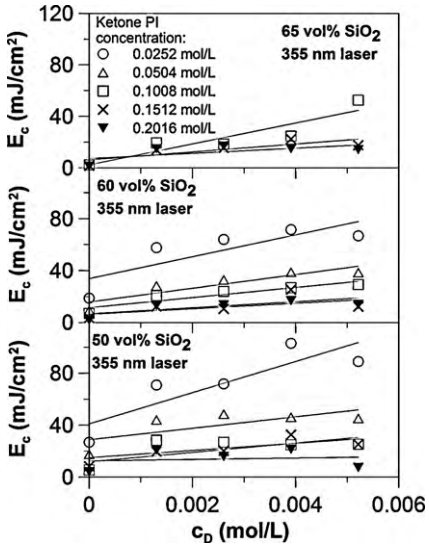

Fig. 6. Critical energy vs. c_D for 50, 60 and 65 vol% SiO_2 suspensions with triazole dye and varying ketone PI concentration (wrt monomer).

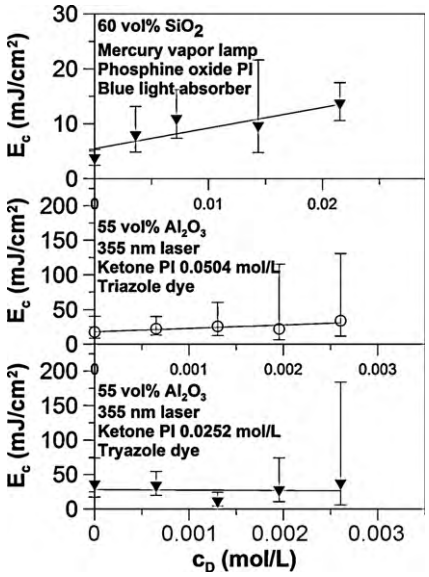

Fig. 7. Critical energy vs. c_D for 60 vol% SiO_2 suspension with phosphine oxide PI and blue light absorber and 55 vol% Al_2O_3 suspension with ketone PI and triazole dye.

The linearized model further predicts that addition of inhibitors should produce a linear curve when E_c is plotted against Q_{added}. Here, we studied the effect of one inhibitor MEHQ and two HALSs that scavenge free radicals and behave similarly as inhibitors as their effect on sensitivity and critical energy. The effect of inhibitor and HALSs on critical energy is shown in Fig. 9 for 60 vol% SiO_2 suspensions with the inhibitor MEHQ, the solid orange HALS and the liquid yellow HALS. The compositions contain ketone PI (0.1008 mol/L wrt monomer). As can be seen from the graph, the data resulted in linear lines, which is in good agreement with the model. The solid orange HALS dramatically increases the critical energy even in small concentrations, while the liquid yellow HALS and MEHQ do not significantly affect the critical energy. Moreover, in case of the liquid yellow HALS the slight increase in the critical energy can be attributed to the reduction of ceramic volume content from 60 to ~56 vol% for a composition with the highest concentration of the liquid yellow HALS, since the HALSs were added after the suspensions were prepared.

Slopes, intercepts and correlation coefficients of the regression lines are summarized in Table 5. The intercept term $I_5 c_P/(1-\Phi)$ reports on the portion of the energy consumed by the native inhibitors and by oxygen inhibition. Its value inferred from the added-inhibitor series was determined to be 2 (mJ-mol)/(L-cm^2). The model predicts that this value should be the same as $I_4 c_P/(1-\Phi)$ from Table 4, which is

Table 4
Actual slopes, intercepts and correlation coefficients of linear regressions E_c vs. c_D for SiO_2 and Al_2O_3 suspensions.

Light source	Ceramic	Φ	PI	c_P (mol/L)	r^2	K_4	I_4	$\frac{K_4 c_P}{(1-\Phi)} = \frac{h\nu}{\Omega}\frac{\gamma_D}{\varepsilon_P}\frac{K_4 c_P}{1-\Phi} = \frac{h\nu}{\Omega}\frac{\gamma_D}{\varepsilon_P}$ (mJ/cm^2)	$\frac{I_4 c_P}{1-\Phi} = \frac{h\nu}{\Omega}(\gamma_Q Q + \gamma_O O)\frac{1}{\varepsilon_P}$ (mJ-mol)/(L-cm^2)
				0.0252	0.85	21,500 ± 14,600	27 ± 6	1100 ± 700	1.36 ± 0.30
				0.0504	0.84	6400 ± 3500	18 ± 3	650 ± 350	1.78 ± 0.28
	SiO_2	0.5	Ketone	0.1008	0.71	5200 ± 1500	6 ± 2	1100 ± 300	1.24 ± 0.43
				0.1512	0.82	5800 ± 2600	9 ± 2	1700 ± 800	2.60 ± 0.65
				0.2016	0.42	3100 ± 1300	5 ± 2	1250 ± 500	1.98 ± 0.80
				0.0252	0.74	14,000 ± 6300	23 ± 10	900 ± 400	1.44 ± 0.66
355 nm laser				0.0504	0.77	6600 ± 2400	11 ± 4	800 ± 300	1.37 ± 0.46
	SiO_2	0.6	Ketone	0.1008	0.83	5600 ± 1900	9 ± 4	1400 ± 500	2.26 ± 0.94
				0.1512	0.69	2000 ± 600	4 ± 1	700 ± 200	1.43 ± 0.39
				0.2016	0.74	3500 ± 500	2 ± 1	1800 ± 300	1.19 ± 0.35
				0.1008	0.87	8900 ± 2000	2 ± 1	2600 ± 600	0.68 ± 0.19
	SiO_2	0.65	Ketone	0.1512	0.75	4400 ± 1300	2 ± 1	1900 ± 600	0.84 ± 0.5
				0.2016	0.78	4100 ± 600	1 ± 0	2400 ± 350	0.71 ± 0.08
Average								1400	1.45
355 nm laser	Al_2O_3	0.55	Ketone	0.0252	−0.13	(−8000) ± 9000	25 ± 12	−450 ± 500	1.42 ± 0.66
				0.0504	0.84	5700 ± 23,900	18 ± 19	600 ± 2700	2.04 ± 2.14
Average									1.73
Mercury vapor lamp	SiO_2	0.6	Phosphine oxide	0.0984	0.87	500 ± 200	4 ± 2	120 ± 50	0.96 ± 0.42

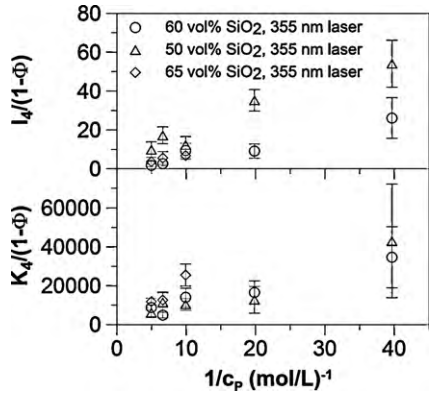

Fig. 8. Slope and intercept determined from linear regressions of E_c vs. c_D for 50, 60 and 65 vol% SiO_2 suspensions.

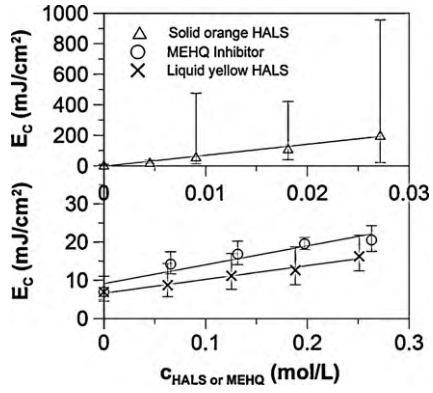

Fig. 9. Critical energy vs. concentration of inhibitor resp HALS (wrt monomer) for ~60 vol% SiO_2 suspension containing the ketone photoinitiator (0.1008 mol/L wrt monomer). Cure depth measurement were performed using the 355 nm laser.

1.45 (mJ-mol)/(L-cm^2) and $K_3/(1-\Phi)$ from Table 2, which is 1.39 (mJ-mol)/(L-cm^2). These are roughly the same. The slope of Fig. 9 is the term $K_5 c_P/(1-\Phi)$, which determines the portion of the energy consumed by the HALSs or the added inhibitor. The portion of the energy absorbed by the solid orange HALS, the liquid yellow HALS and inhibitor MEHQ was estimated to be 1033 ± 756, 12 ± 4 and 9 ± 6 mJ/cm^2, respectively.

The model further predicts that the E_c is a linear function of ceramic volume fraction Φ. Shown in Fig. 10 is the E_c vs. Φ for 50–65 vol% suspensions including compositions with silica and alumina ceramics. These data can be reasonably represented by straight lines. The slopes, intercepts and correlation coefficients are shown in Table 6. The slope term $K_6 c_P$ should be numerically equal to (but opposite in sign) to the intercept term $I_6 c_P$. The

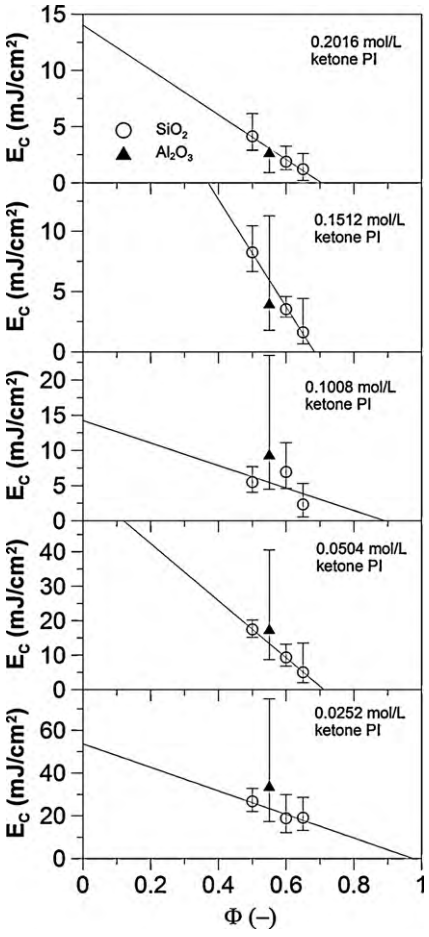

Fig. 10. E_c vs. Φ for SiO_2 and Al_2O_3 suspensions with varying concentration of ketone PI (wrt monomer) and no dye. Cure depth measurements were performed using 355 nm laser

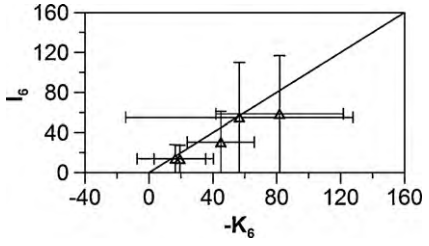

Fig. 11. Intercepts I_6 vs. slopes ($-K_6$) determined from plots E_c vs. Φ. The data appears in Table 6.

slope term and intercept term are approximately similar. Fig. 11 shows the plot of the intercept I_6 vs. the slope $-K_6$.

Table 5
Actual slopes, intercepts and correlation coefficients of linear regressions E_c vs. Q_{added} for ~60 vol% SiO_2 suspensions with ketone PI (0.1008 mol/L wrt monomer). The cure depth measurements were performed using 355 nm laser.

	r^2	K_5	I_5	$\frac{K_5 c_P}{1-\Phi} = \frac{h\nu}{\Omega}\frac{\gamma_{Q,added}}{\varepsilon_P}\frac{K_5 c_P}{(1-\Phi)} = \frac{h\nu}{\Omega}\frac{\gamma_{Q,added}}{\varepsilon_P}$ (mJ/cm^2)	$\frac{I_5 c_P}{1-\Phi} = \frac{h\nu}{\Omega}(\gamma_{Q,native} Q_{native} + \gamma_O O)\frac{1}{\varepsilon_P}$ (mJ-mol)/(L-cm^2)
Solid orange HALS	0.98	4100 ± 3000	7 ± 4	1033 ± 756	1.76 ± 1.01
Inhibitor MEHQ	0.87	49 ± 16	10 ± 3	12 ± 4	2.52 ± 0.76
Liquid yellow HALS	0.98	36 ± 25	7 ± 4	9 ± 6	1.76 ± 1.01
Average					2.01

Table 6
Actual slopes, intercepts and correlation coefficients of linear regressions E_c vs. ceramic volume content Φ. The suspensions contain ketone PI (mol/L wrt monomer) and no dye and cure depth measurements were performed using 355 nm laser.

c_P (mol/L)	r^2	K_6	I_6	$-K_6c_P = \frac{h\nu}{\Omega}(\gamma_Q Q + \gamma_O O)\frac{1}{\varepsilon_P} - K_6c_P = \frac{h\nu}{\Omega}\left(\gamma_Q Q + \gamma_O O\right)\frac{1}{\varepsilon_P}$ (mJ-mol)/(L-cm^2)	$I_6c_P = \frac{h\nu}{\Omega}(\gamma_Q Q + \gamma_O O)\frac{1}{\varepsilon_P}$ (mJ-mol)/(L-cm^2)
0.0252	0.78	−57 ± 71	55 ± 40	1.4 ± 1.8	1.4 ± 1.0
0.0504	0.99	−82 ± 40	59 ± 22	4.1 ± 2.0	2.9 ± 1.1
0.1008	0.11	−16 ± 24	14 ± 14	1.7 ± 2.4	1.4 ± 1.4
0.1512	0.97	−45 ± 21	31 ± 12	6.8 ± 3.2	4.6 ± 1.9
0.2016	0.97	−19 ± 16	14 ± 10	3.9 ± 3.3	2.8 ± 2.0
Average				3.6	2.6

The first level predictions of the linearized inhibitor exhaustion model were that the E_c should increase linearly with the inverse of the photoinitiator concentration ($E_c \sim 1/c_P$), and increase linearly with the inert dye concentration ($E_c \sim c_D$), increase linearly with added inhibitor ($E_c \sim Q_{added}$). These are in good agreement with the observations, as we find good linear correlations. The agreement covers a rather wide parameter space, with E_c ranging over a factor of 5 or more, with photoinitiator concentration varied by a factor of 8 and dye concentration varying by a factor of 5, using two UV sources, and different photoactive additions. Ceramic volume fraction varied over rather narrower ranges, and is in rough agreement with what is expected from the linear model. These are based on E_c values obtained from fitting the cure depth-energy dose raw data to the Jacob's equation. The second level of predictions, which involve the slopes and intercepts for E_c vs. c_D, and $1/c_P$, are also in reasonable agreement with the observations, although with more scatter and variation. This is not surprising, since the slopes and intercepts are inferred from regression lines fit to predictions from the linearized model. On the whole, the prediction of this simple linearized model is well supported by our observations.

3.1. Predicted vs. observed critical energy

Of course the value of the model is to predict critical energy from the composition of the photosuspension. As indicated in the introduction, terms in Eqs. (3)–(6) for the slopes and intercepts appear repeatedly, so each independent series of experiments provides another estimate for the value for these collections of terms. The collection terms obtained from the complete set of many experiments are summarized in Table 7. The average values were used to obtain a set of "predicted" E_c values for ∼100 different individual compositions. The predicted critical energy values for many different individual resin compositions are compared in Fig. 12 with experimental E_c values. For clarity, most of the data are presented only as $E_{c\,average}$. A few of experimental values also show with the uncertainly ranges $E_{c\,min}$ and $E_{c\,max}$. The linearized model overestimates the critical energy for many

Table 7
Collection terms for the portion of energy consumed by the inhibitor and the portion of the energy consumed by the dye.

Collection term	Plot E_c vs.	Eq.	Light source	Suspensions	PI	Dye	
$\frac{h\nu}{\Omega}(\gamma_Q Q + \gamma_O O)\frac{1}{\varepsilon_P}\frac{h\nu}{\Omega}\left(\gamma_Q Q + \gamma_O O\right)\frac{1}{\varepsilon_P}$ (mJ-mol)/(L-cm^2)	$1/c_P$	K_3	355 nm laser; mercury vapor lamp	SiO_2; Al_2O_3	Ketone	–	1.39
	c_D	I_4	355 nm laser	SiO_2	Ketone	Triazole dye	1.45
	c_D	I_4	355 nm laser	Al_2O_3	Ketone	Triazole dye	1.73
	Q_{added}	I_5	355 nm laser	SiO_2	Ketone	–	2.01
Average used in Fig. 12							1.65
$\frac{h\nu}{\Omega}(\gamma_Q Q + \gamma_O O)\frac{1}{\varepsilon_P}\frac{h\nu}{\Omega}\left(\gamma_Q Q + \gamma_O O\right)\frac{1}{\varepsilon_P}$ (mJ-mol)/(L-cm^2)	Φ	K_6	355 nm laser	SiO_2; Al_2O_3	Ketone	–	3.6
	Φ	I_6	355 nm laser	SiO_2; Al_2O_3	Ketone	–	2.6
Average							3.1
$\frac{h\nu}{\Omega}(\gamma_Q Q + \gamma_O O)\frac{1}{\varepsilon_P}\frac{h\nu}{\Omega}\left(\gamma_Q Q + \gamma_O O\right)\frac{1}{\varepsilon_P}$ (mJ-mol)/(L-cm^2)	$1/c_P$	K_3	Mercury vapor lamp	SiO_2	Phosphine oxide	–	0.89 ± 0.12
	c_D	I_4	Mercury vapor lamp	SiO_2	Phosphine oxide	Blue light absorber	0.96 ± 0.42
Average used in Fig. 12							0.93
$\frac{h\nu}{\Omega}\frac{\gamma_D}{\varepsilon_P}\frac{h\nu}{\Omega}\frac{\gamma_D}{\varepsilon_P}$ (mJ/cm^2)	$1/c_P$	K_3	355 nm laser	SiO_2	Ketone	Triazole dye	1530
	c_D	K_4	355 nm laser	SiO_2	Ketone	Triazole dye	1400
Average used in Fig. 12							1465

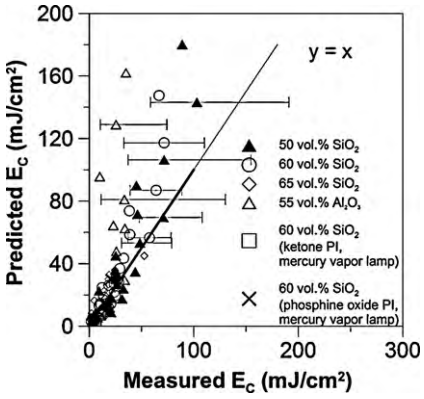

Fig. 12. Predicted E_c vs. measured E_c for 50, 60 and 65 vol% SiO_2 suspensions and 55 vol% Al_2O_3 suspension. The suspensions contained ketone PI and cure depth measurements were performed using the 355 nm laser unless otherwise specified.

of the alumina suspensions. For the silica suspensions most of the predicted E_c fall within 20% of the experimental $E_{c\,average}$. Many of the predicted values are larger than the experimental values, but the large uncertainty range of the experimental E_c values obscures more detailed comparison. The linearized model is able to predict E_c within about 20% suspensions with E_c values smaller than 50 mJ/cm^2. The critical energy for compositions with larger concentrations of dye or inhibitor, where the measured E_c is larger than 50 mJ/cm^2, are consistently overestimated by the model. The model assumes that the fraction of photons which are absorbed by the PI to create free radicals is the PI attenuation length divided by the total attenuation length for PI absorption, dye absorption, and scattering, as described by Eq. (20) in the previous paper.[6] Perhaps this is less accurate for dye-dominated or scattering-dominated suspensions, which tend to have higher E_c. If this approximation under-estimates the fraction of photons absorbed by PIs, the model would overestimate E_c for these cases.

4. Conclusions

The critical energy dose E_c, inferred from measurements of cure depth as a function of energy dose, is inversely proportional to the photoinitiator concentration for ketone and phosphine oxide photoinitiators in acrylate monomer with dispersed silica or alumina powders. Inert UV absorbing dyes increase the critical energy dose, with E_c directly proportional to the dye concentration. The critical energy is directly proportional to the concentration of quinone inhibitor and hindered amine inhibitors. These results agree with the predictions of the model that presumes that E_c is the energy dose that produces sufficient free radicals to exhaust native inhibitors. A linearized form of this model predicts linear behavior for E_c vs. the inverse of the photoinitiator concentration, for E_c vs. dye concentration, for E_c vs. inhibitor concentration, and for E_c vs. ceramic volume fraction. Experiments confirmed these predictions, and provided a self-consistent set of parameters from the slopes and intercepts of the lines.

Values for E_c predicted from the model using these parameters agreed satisfactorily for E_c values below about 50 mJ/cm^2, but overestimate E_c for suspensions with larger critical energy.

Acknowledgements

This research was supported by the United States Defense Advanced Research Projects Agency (DARPA) under HR0011-07-1-0034, Program Officer W. S. Coblenz and the Office of Naval Research under N00421-06-1-002, Program Officer David Shifler.

References

1. Ebert J, Özkol E, Zeichner A, Uibel K, Weiss Ö, Koops U, et al. Direct inkjet printing of dental prostheses made of zirconia. *J Dent Res* 2009;**88**(7):673–6.
2. Doreau F, Chauput C, Chartier T. Stereolithography for manufacturing ceramic parts. *Adv Eng Mater* 2000;**2**(8):493–6.
3. Provin C, Monneret S. Complex ceramic–polymer composite microparts made by microstereolithography. *IEEE Trans Electron Pack Manuf* January 2002;**25**(1).
4. Lee JH, Prud'homme RK, Aksay IA. Cure depth in photopolymerization: experiments and theory. *J Mater Res* 2001;**16**:3536–44.
5. Jacobs PF. Rapid prototyping & manufacturing—fundamentals of stereolithography. *Soc Manuf Eng* 1992.
6. Tomeckova V, Halloran JW. Predictive models for the photopolymerization of ceramic suspensions. *J Eur Ceram Soc* 2010;**30**:2833–40.
7. Tomeckova V, Halloran JW. Cure depth for photopolymerization of ceramic suspensions. J Eur Ceram Soc; doi:10.1016/j/jeurceramicsoc.2010.06.004, in press.
8. Fouassier J-P. *Photoinitiation, photopolymerization, and photocuring: fundamentals and applications*. Munich: Hanser Gardner Publications; 1995.
9. Garg R, Prud'homme RK, Aksay IA, Liu F, Alfano RR. Absorption length for photo propagation in highly dense colloidal dispersions. *J Mater Sci* 1998;**13**(12):3463–7.
10. Wu KC, Seefeldt KF, Solomon MJ, Halloran JW. Prediction of ceramic stereolithography resin sensitivity from theory and measurement of diffusive photon transport. *J Appl Phys* July 2005;**98**:024902-1–10.